doi:10.36487/ACG_repo/2063_31

Physical modelling to provide data-rich case studies for the verification and validation of numerical modelling predictions of cave mechanics problems

J Wesseloo Australian Centre for Geomechanics, The University of Western Australia, Australia

D Cumming-Potvin Australian Centre for Geomechanics, The University of Western Australia, Australia

Y Potvin Australian Centre for Geomechanics, The University of Western Australia, Australia

SW Jacobsz The University of Pretoria, South Africa

E Kearsley The University of Pretoria, South Africa

Abstract

Due to the nature of cave mining, the industry needs to rely on indirect data and limited direct observation to investigate the mechanisms and processes of cave propagation. A collaborative project with the Australian Centre for Geomechanics, the University of Western Australia, and the Department of Civil Engineering, University of Pretoria was initiated to study these processes in the laboratory using geotechnical centrifuge modelling. The results of the first phase of this study postulated a discontinuous caving process with fracture banding occurring (Cumming-Potvin 2018; Cumming-Potvin et al. 2016a). A second phase of the project has been initiated under the sponsorship and in collaboration with Newcrest Mining Ltd. Several improvements to the experimental setup were introduced in the second phase with several further tests performed. The mechanism of cave propagation in the centrifuge is dominated by extension fracturing initiating in the cave crown and extending parallel to the cave back, with secondary shear fractures predominantly occurring on the side of the cave closer to the abutment.

1 Introduction

Cave propagation is a complex geomechanical process influenced by geological, geotechnical, structural geological and mining factors. Access to the caving column is limited and, as a result, modelling of cave propagation is a data-limited exercise with associated uncertainty ensuing. Due to the restricted access to the caving column during the whole mine life, interpretation of the rock mass behaviour is, by necessity, limited to inference from indirect instrumentation methods, such as seismic assessment and direct point measurements with limited spatial coverage, like observation holes, extensometers, TDRs, smart markers, etc. As a result, our fundamental understanding of caving geomechanics is limited. It is generally accepted that every cave is unique, but they all have common threads.

The geomechanics of cave mining is concerned with a wide range of rock mass behaviour from the small strain elastic range to the phase change from fractured continuum to a particulate medium subject to granular flow. For design purposes, it is necessary to reliably model the full range of material behaviour with further complexities (for example, the presence of major faults or geological contacts) superimposed onto the problem.

Numerical modelling has become a widely used tool in the geomechanical design of cave mines. These models are used to predict the expected behaviour under assumed design conditions. During the construction and operation of the mine, these models are often used to provide the predictions based on which design parameters and management decisions are made.

In his Rankine Lecture, Lambe (1973) suggested five different prediction classes. The distinction between the different prediction classes is important for further discussion (refer to Table 1).

Table 1 Lambe's classification of prediction

Prediction type	When prediction was made	Results at the time prediction was made
A	Before event	-
B	During event	Not known
C	After event	Not known
B1	During event	Known
C1	After event	Known

Numerical modelling performed as part of a Block and Panel caving mine design can be regarded as a Class A prediction. Class A predictions are, therefore, extremely important to industry. Due to the large capital investment associated with cave mining operations, the financial risk associated with the model uncertainty is large, and an understanding of the accuracy, reliability and applicability of the modelling methodology in Class A predictions is important.

The literature contains the results of more type C1 predictions than of any other type. For example, many articles discuss some form of calibration where the model input parameters are adjusted to reproduce known results. This is also the case for caving geomechanics. However, these class C1 models rely on uncertain interpretation of indirect monitoring with limited direct measurements, and the known results are themselves subject to uncertain interpretation. Class C1 prediction is, therefore, extremely important in advancing our understanding of the problems that we try to model. However, Lambe (1973) points out that:

> *"…one must be suspicious when an author uses type C1 predictions to 'prove' that any prediction technique is correct…"*

And later in the same lecture:

> *"Most engineering decisions and actions must be based on type A predictions, and sometimes on type B predictions. However, most evaluations of prediction techniques are based on type C and type C1 predictions."*

Since numerical modelling plays such an important role in cave mining, it is of utmost importance that these models are validated and calibrated with data-rich problems.

The lack of data-rich caving problems for the calibration/validation of both the numerical models and the indirect monitoring used to calibrate/validate these models lead to model uncertainties. One important question in this regard is whether the modelling method and material model have the intrinsic ability to mimic or represent all the different mechanisms that could be manifest, or does the model have a bias towards a specific mechanism? These uncertainties translate into risk when models are used as class A predictions. The difficulty with validation and calibration of numerical models in a data-poor environment is conceptually illustrated in Figure 1.

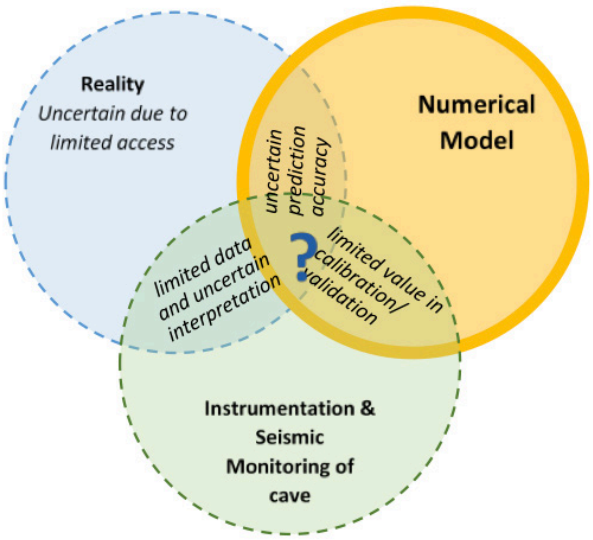

Figure 1 Schematic highlighting the lack of knowledge on caving geomechanics

2 Physical modelling

Physical modelling is a relatively easy and cost-effective way to produce data-rich environments for the calibration and validation of modelling approaches and methods as it can be instrumented and visually inspected in a way not possible in a real cave (Figure 2).

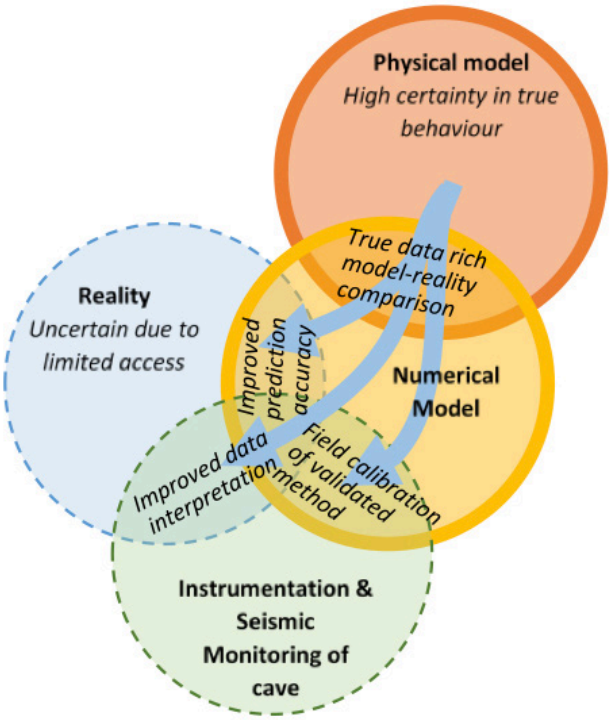

Figure 2 Addressing knowledge gaps through the use of physical modelling

In hydrological studies, physical models are used very effectively to replicate specific real-life scenarios (e.g. Güney et al. 2014; Kumcu 2017; Torres Mansilla 2018). This is also often the case in some soil mechanics problems (refer to series of proceedings of the International Conference on Physical Modelling in Geotechnics (ICPMG)). It is, however, not practically possible to replicate a specific real cave. The value of physical models for caving scenarios lies in the fact that the failure mechanisms involved in the caving

process can be studied in a data-rich environment. Physical modelling can be used to validate numerical approaches and/or lead to their improvement when some of the important mechanisms are not captured by specific modelling approaches.

3 Why use a centrifuge?

The first question to answer is why it is necessary to use a centrifuge at all, as it creates a more complicated and expensive experimental setup. For problems where gravity loading influences the behaviour, the use of a centrifuge is necessary to replicate true behaviour at a smaller scale. This is illustrated in the following example.

Consider the two-dimensional scenario illustrated in Figure 3 with a vertical-sided block undercut by a larger excavation.

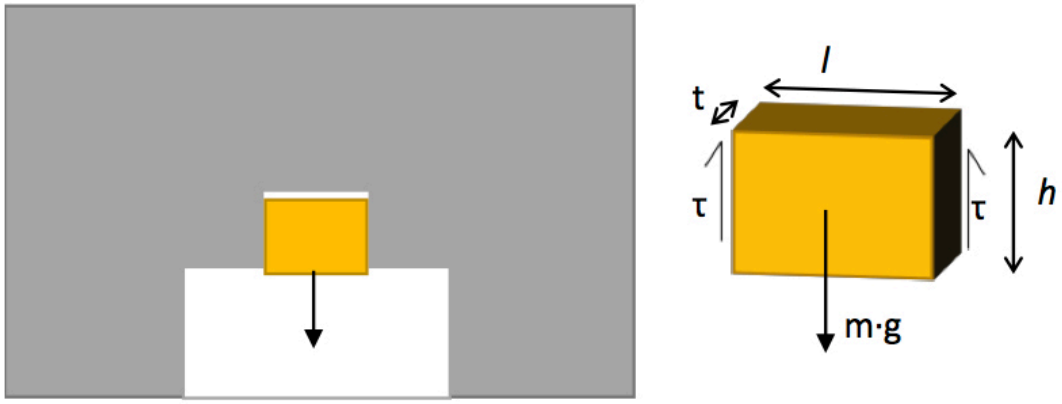

Figure 3 Conceptual scenario of potentially unstable block in the roof of an excavation

For the block to fall out, the downward gravitational force needs to be greater than the upwards-stabilising shear strength of the vertical sides of the block, i.e.:

$$2 \cdot \tau \cdot (t \cdot h) \leq (l \cdot t \cdot h) \cdot \rho \cdot g \quad (1)$$

Where:

τ = the shear stress on the side of the block

ρ = the material density

l, t, h = the three dimensions of the block

g = gravitational acceleration

which we can write in the standard form of a Factor of Safety (FS)(capacity divided by demand) as:

$$FS = \frac{2 \cdot \tau}{l \cdot \rho \cdot g} \leq 1 \quad (2)$$

For illustration purposes, let us assume the shear strength on the two sides is 100 kPa and the density of the block is 2,800 kg/m^3. For this example, the FS of a 7.3 m wide block is just less than one, and therefore, the block is predicted to drop out.

Building a laboratory-scale model out of the same material at a scale of 1:100, we will have a 7.3 cm wide block with an FS of approximately 100, and the model will not replicate the true behaviour. The only way to have the model replicate the true behaviour is to increase the gravitational acceleration until the FS again reaches 1, i.e. increasing the gravitational acceleration by a factor of 100. For this example, the same behaviour will be achieved for any model with the same value for the product $l \cdot g$.

For illustration purposes, the strength of the block sides was kept constant. For strong materials, high enough centrifugal acceleration may not be achievable, making it necessary to also scale down the strength of the material. An equivalent scale model can be achieved by scaling different parameters by different factors as follows:

$$\frac{2\cdot(f_\tau\cdot\tau_m)}{l\cdot(f_\rho\cdot\rho)(f_g\cdot g)} = \frac{2\cdot\tau}{l\cdot\rho\cdot g} \tag{3}$$

Geotechnical research with the use of centrifuge physical modelling is fairly common in the civil engineering industry. It is interesting to note, however, that the world's first geotechnical centrifuge was developed for the use of studying mining-related problems (Bucky 1931; Bucky & Fentress 1934; Bucky et al. 1935). Evert Hoek (1965) built a geotechnical centrifuge at the CSIR in South Africa and studied problems related to deep mining in South Africa at the time. Figure 4 and Figure 5 show some of the results from this work and illustrate the importance of the use of centrifugal scaling of the laboratory model. In both figures, the left-hand side sub-figure (a) shows the model results without the centrifugal loading and the right-hand side (b), with centrifugal loading. Figure 4 shows the photoelastic contours of strain in the model. These models include pillars in thin tabular excavations. Figure 4 illustrates the large difference in the fracture patterns and the failure mechanism that develops for duplicate models without and with the inclusion of the scaled gravitational loading.

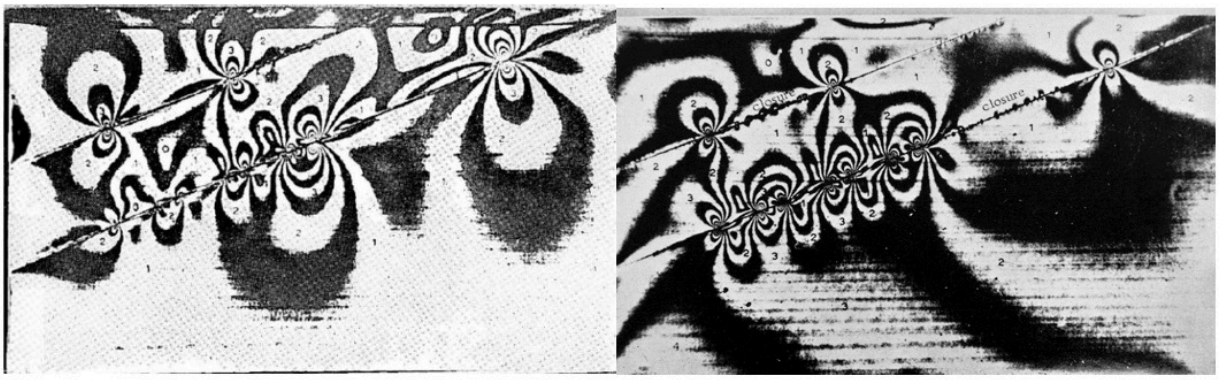

a) 1g test b) 100g test

Figure 4 Comparison between photoelastic patterns under a) uniformly distributed loading, and b) with the addition of body force loading (Hoek 1965)

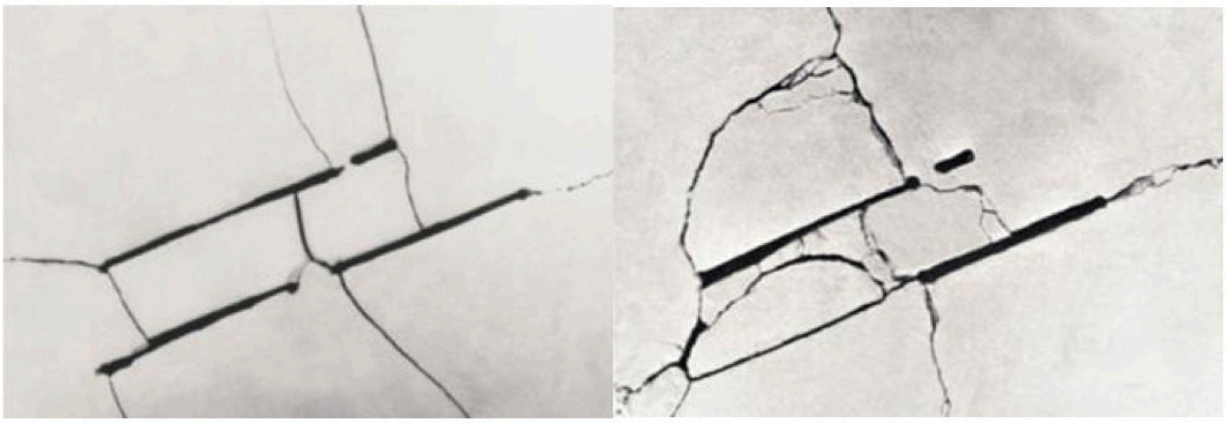

b) 1g test b) 600g test

Figure 5 Fracture patterns showing the importance of body forces in the fracture of large rock masses under a) uniformly distributed loading, and b) with the addition of body force loading (Hoek 1965)

4 Centrifugal models of caving mechanics

Brown (2007) points out that the mechanism by which caving occurs is dependent on the relationship between the stresses induced by mining activities, the geometry of the rock mass, and the strength of the discontinuities in the rock mass. Brown points out that the propagation of caving in low stress environments requires the presence of a well-developed low-dip discontinuity set. Gravity caving occurs when the tangential induced stress in the crown is tensile or exhibits low compression allowing rock blocks to fall freely under gravity (Brown 2007). When the tangential stress is high compared to the compressive strength of the rock mass stress, caving occurs as a result of the failure of intact rock (Brown 2007) and the rock mass damage creating blocks that could be mobilised under gravity.

In 2014, the Australian Centre for Geomechanics at the University of Western Australia, in collaboration with the Department of Civil Engineering at the University of Pretoria, embarked on a physical modelling programme to study the mechanics of cave propagation under stress caving conditions where compressive horizontal stresses are induced in a material without a low-dip discontinuity set. The most important results from the first phase are summarised in Section 4.1, with more detail available in several previous publications (Cumming-Potvin 2018, Cumming-Potvin et al. 2016a, 2016b, Jacobsz et al. 2018).

4.1 Phase 1

During the first phase of physical modelling of the cave mechanics, the observed damage propagation mechanism differed from that envisaged in Duplancic's conceptual model of caving propagation (Duplancic & Brady 1999). The Duplancic model assumes a continuous damage profile whereby the rock mass ahead of the cave transitions gradually from intact rock mass to a seismogenic zone through to yielded rock mass and mobilised rock. The mechanism observed in the centrifuge had a discontinuous damage profile, with a series of fractures oriented sub-parallel to the cave surface. The cave back progressed by jumps to the next successive parallel fracture. This caving mechanism was termed 'fracture banding.' Figure 5 presents one of several tests where it could be seen that the fracture termination point is influenced by the piston dimensions at the region of the piston. It is important to note the abundant cases in which the fracture banding occurs where the piston dimensions plays no role. This is evident, for example, in Figure 6 F to H where the fracture banding continues to occur without any further possible influence from the discontinuous piston retraction.

Cumming-Potvin also observed the signature of fracture banding from seismic monitoring at a number of mine sites (Figure 7). Furthermore, a period of rapid cave propagation with little seismicity ahead of the cave back was observed through open hole monitoring – indicating a fracture banding mechanism (Figure 8, Area 2). This transitioned to a period with more seismicity and significant shear damage ahead of the cave back, indicating a change to a Duplancic mode of caving (Figure 8, Area 3).

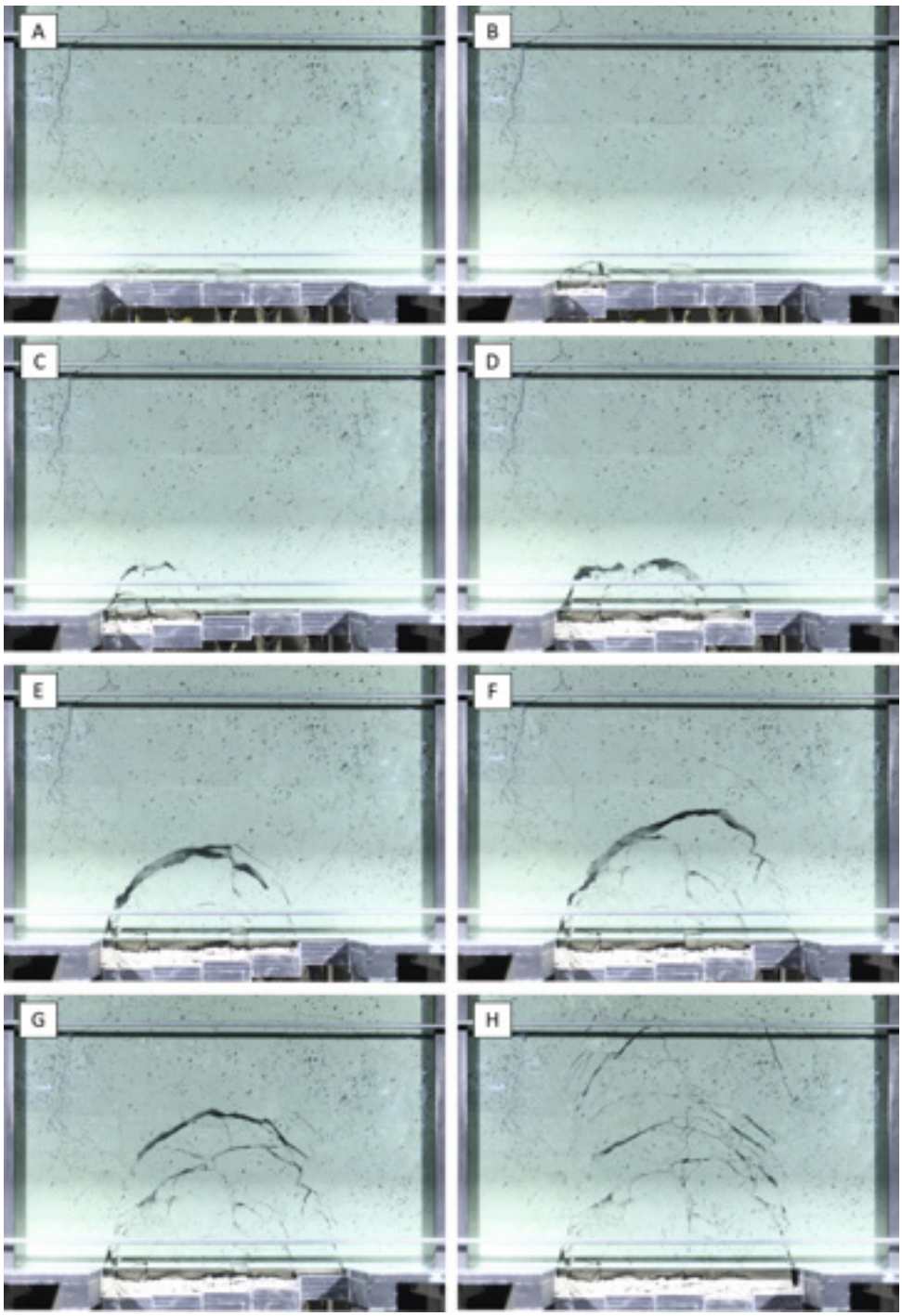

Figure 6 **Example of centrifuge modelling of cave propagation showing fracture banding (Cumming-Potvin 2018)**

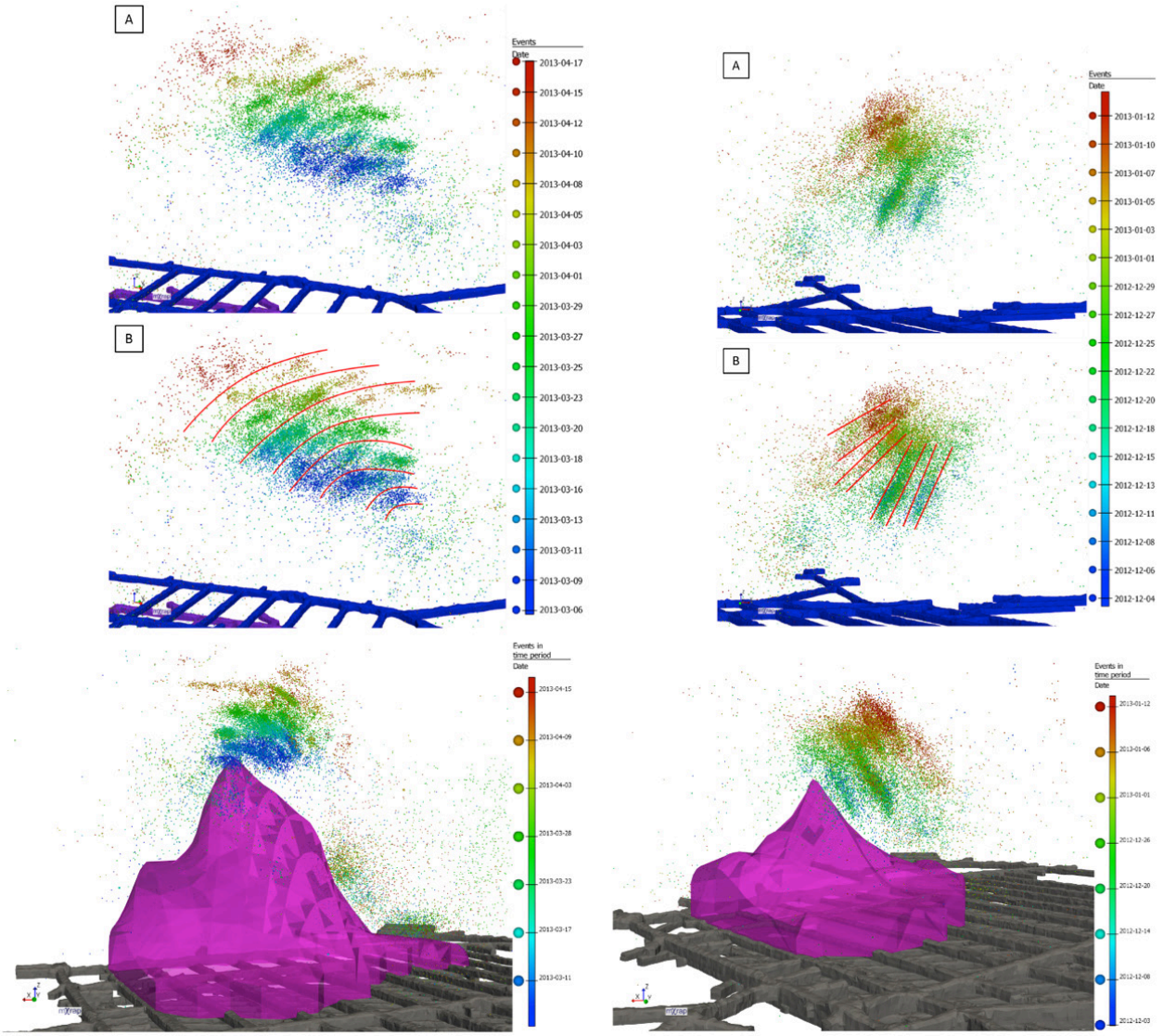

Figure 7 Examples of seismic events forming bands that jump up vertically with time (seismic events coloured by time) (Cumming-Potvin 2018)

Cumming-Potvin (2018) concluded that the Duplancic model may not cover the full range of possible mechanisms of cave propagation and that it required extension. An expanded model of caving mechanics was proposed, which could capture both fracture banding and the Duplancic mode of caving (Figure 9).

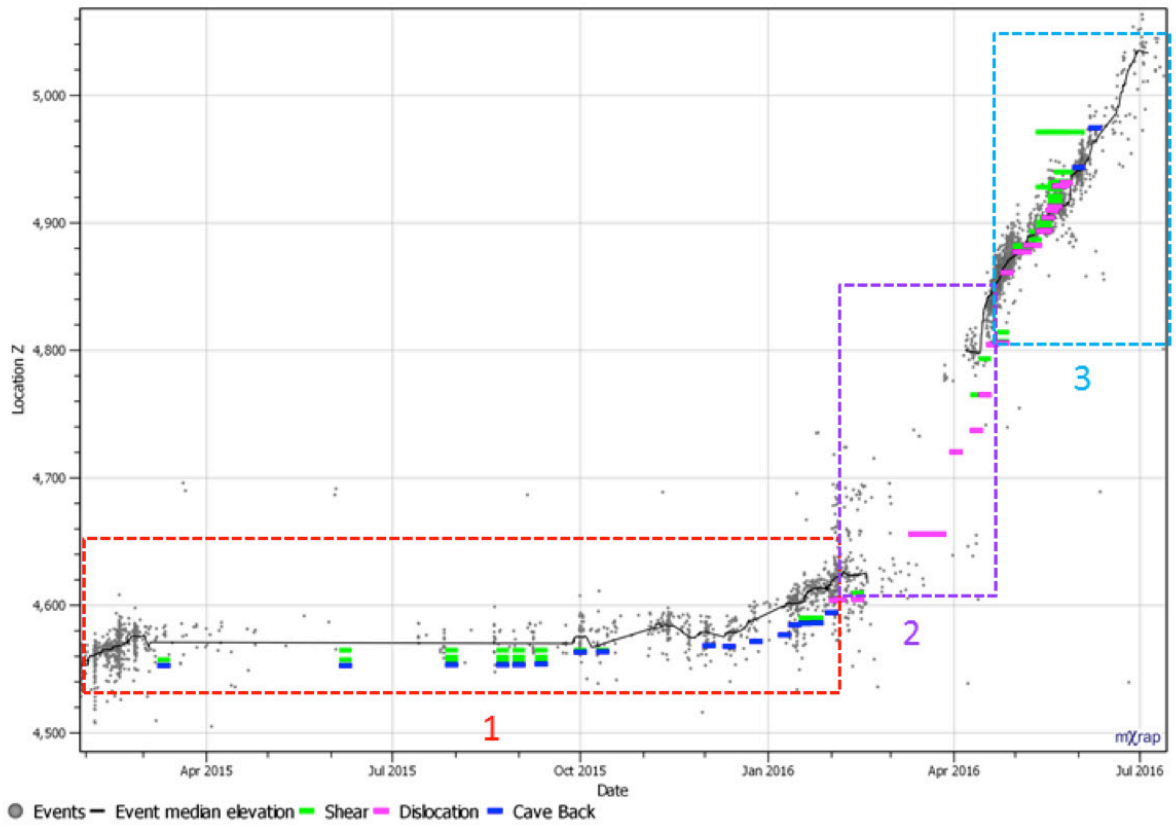

Figure 8 **Example from a caving mine of cave initiation (Area 1 in red), fracture banding (Area 2 in purple), then a transition to a Duplancic mode of caving (Area 3 in blue) (Cumming-Potvin 2018)**

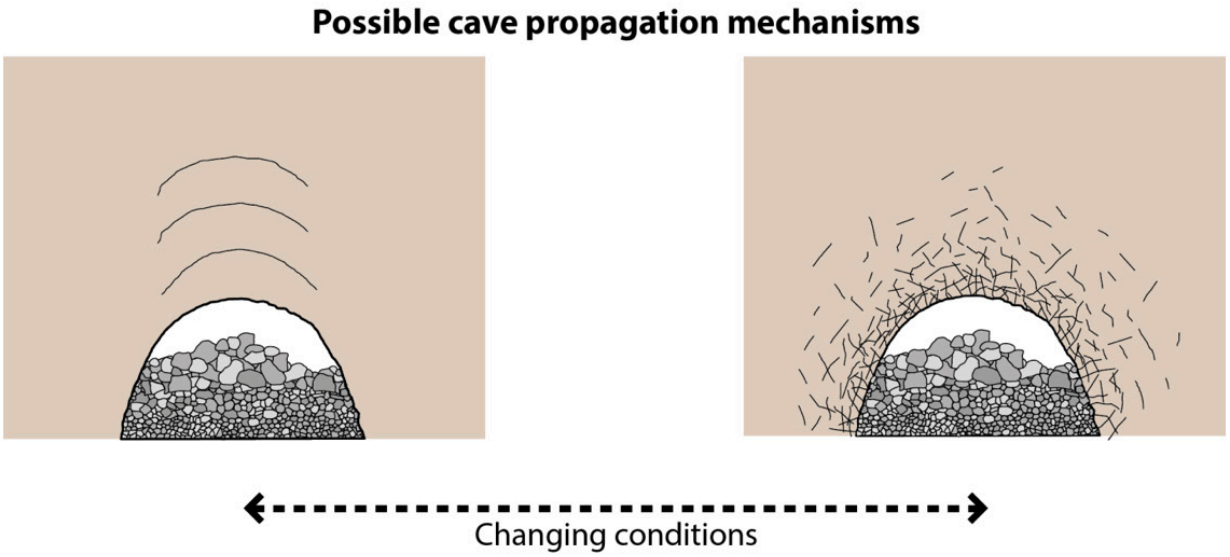

Figure 9 **Expanded model of caving mechanics (Cumming-Potvin 2018)**

4.2 Phase 2

With the experience gained from the first phase of testing, several improvements were made to the test setup. These included improving the test frame, the testing material, instrumentation and testing procedures. The test configuration used in the second testing phase is presented in the following sections.

4.2.1 Test frame

The test frame shown in Figure 10 is largely constructed with aluminium and accommodates a sample of up to 450 mm high by 500 mm wide by 50 mm thick. Cavities on both sides of the sample space house rubber bladders used to impose gravity-induced horizontal pressure onto the sample.

Since the testing is performed on a thin sample slab, it is important to maintain a good reactive confinement in the out-of-the-plane direction. The back plate was stiffened with 25 mm wide by 50 mm deep horizontal and vertical webbing, spaced at 125 mm intervals. The front of the sample is confined with 3 plates of 10 mm thick tempered low iron glass laminated together to form one pane. Although the aim was to generate plane strain conditions, the confinement stress generated on the back plate could not be measured in the test to confirm this, and it is expected that full plane strain conditions may not have been achieved.

Figure 11 illustrates the intended stress conditions aimed for in the physical model. Due to the horizontal stress induced by the bladders and the vertical stress relaxation due to the cave void, the major principal stress above the cave back is horizontal in the plane of the sample. The minor and intermediate stress is expected to act vertically and horizontally onto the plane of the sample. At the cave back, this vertical stress reduces to zero with the induced horizontal stress across the plane of the sample being the intermediate principal stress.

a) Test sample in frame **b) stiffened back of frame** **c) assembled frame with sample**

Figure 10 Test frame with sample

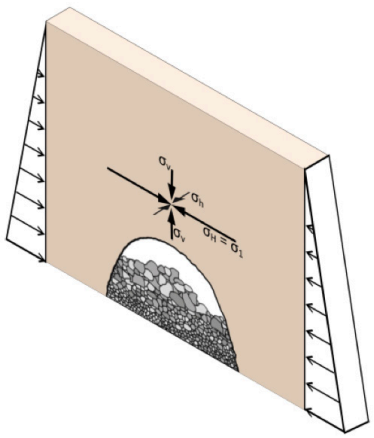

Figure 11 Intended induced stress state in the cave back

4.2.2 Undercutting arrangement

The undercutting of the sample was performed with five SFX 1000 N actuators with a 100 mm full stroke. Electrical actuators provide a stiff system with easy and precise control compared to the hydraulic pistons used in the earlier tests.

4.2.3 Visual recording

Visual recording of the propagation was performed with three on-board cameras. A webcam provided live visual feedback throughout the test and the video feed was recorded during the test. A Canon EOS 100D with a 40 mm fixed lens camera was mounted on the centrifuge and took photographs at intervals of 5 seconds.

Higher speed images are necessary to study the propagation mechanism, e.g., to determine the mode of crack formation and the location of crack initiation. For this purpose, 2 MP grey-scale images were recorded at 10 ms intervals. These images were recorded with a Basler acA2000-165uc USB 3.0 camera fitted with an 8.5 mm F/1.3-16 lens. A dedicated on-board computer recorded the images from the camera.

4.2.4 Acoustic emissions recording

A total of 10 single element 1 MHz contact transducers were used to record acoustic emissions. Five of these are longitudinal wave transducers and the other five are transverse wave transducers. For clear separation of the first wave arrivals, a high sampling rate is required. Continuous monitoring at a sampling frequency of 96 kHz was performed throughout the tests.

On the two sides of the sample, longitudinal wave sensors were placed within sensor guides between the bladders and the sample, with the lateral pressure from the bladders ensuring contact between the sensors and the sample. A sensor guide with the longitudinal wave sensors was placed on top of the sample with small weights on top of the sensors ensuring contact between the sensor and the sample. The transverse wave sensors were installed from the back of the sample through holes in the backplate and kept in contact with the sample through a spring load system. The analysis of the acoustic emissions data was, however, outside the scope of this paper.

4.2.5 Model material

The illustration of the stability of a vertical-sided block was used in Section 3 to illustrate the necessity for scaling up the gravitational loading to induce realistic behaviour of laboratory models under gravitational loading. For simplicity, the strength of block sides in the example was kept constant. As mentioned before, for strong materials, however, high enough centrifugal acceleration may not be achievable in the laboratory, making it necessary to also scale down the strength of the material. The scaling of the model can be achieved by scaling different parameters. To extend the previous example, scaling can be achieved as follows with the left-hand side of the equation indicating the FS of the block in the laboratory experiment and the right-hand side the FS of the large-scale situation being modelled. For this particular example, the in-situ behaviour can be replicated. The scaling can be achieved by:

$$\frac{2 \cdot \tau_m}{l_m \cdot \rho_m \cdot g_m} = \frac{2 \cdot \tau}{l \cdot \rho \cdot g} \tag{4}$$

$$\frac{2 \cdot (f_\tau \cdot \tau)}{(f_l \cdot l) \cdot (f_\rho \cdot \rho)(f_g \cdot g)} = \frac{2 \cdot \tau}{l \cdot \rho \cdot g} \tag{5}$$

Where:

τ_m, τ = the shear stress for the model and the modelled scenario respectively

ρ_m, ρ = the model and modelled material density

l_m, l = the model and modelled scale

g_m = gravitational acceleration in the model

g = gravitational constant ≈ 9.8m/s^2

f_l, f_ρ, f_g, f_τ scaling factors for the different parameters

For this particular example, the large scale behaviour can be replicated in the laboratory for any model where:

$$\frac{f_\tau}{f_l \cdot f_\rho \cdot f_g} = 1 \tag{6}$$

For the physical modelling of cave initiation and propagation at 100 g acceleration, it is necessary to scale down the material strength. A fairly weak and brittle model material was achieved after some experimentation with a mixture of kaolinite, fly ash and water. After mixing, the material was placed in a mould and vibrated on a vibrating table. Following the initial setting, the sample was placed in an oven at 70°C for 48 hours and left to cure for another 11 days at room temperature.

The mechanical properties of the test material are summarised in Figure 12 presenting results from uniaxial, triaxial and Brazilian tensile tests. The Brazilian tensile tests do not induce uniaxial tensile conditions, and the test results are plotted at the appropriate induced stress state in the sample.

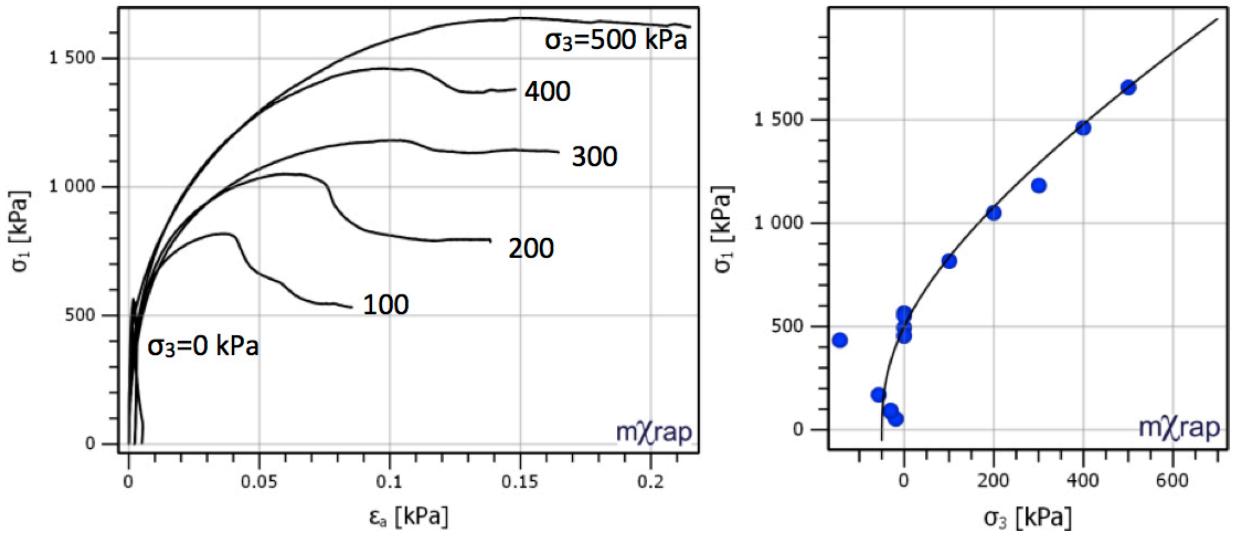

Figure 12 Compressive and tensile strength behaviour of model material

Similar to rock, the model material fails in a brittle manner under low confinement with an increase in ductility with higher confinement. The angularity and aspect ratio of the fragments also resemble that of fragmented rock (Figure 13).

4.2.6 Test procedure

After preparation of the test setup and instrumentation, the centrifuge was accelerated to 80 g before any undercutting commenced. Undercutting of the sample was performed by retracting the actuators in sequence from one side to the other. Caved material was retained on top of the actuator during the test, and cave draw was represented by continual retraction of the actuator.

When the cave stalled after all the actuators were retracted, the actuators were kept at the same level and the centrifugal acceleration increased until caving was reinitiated.

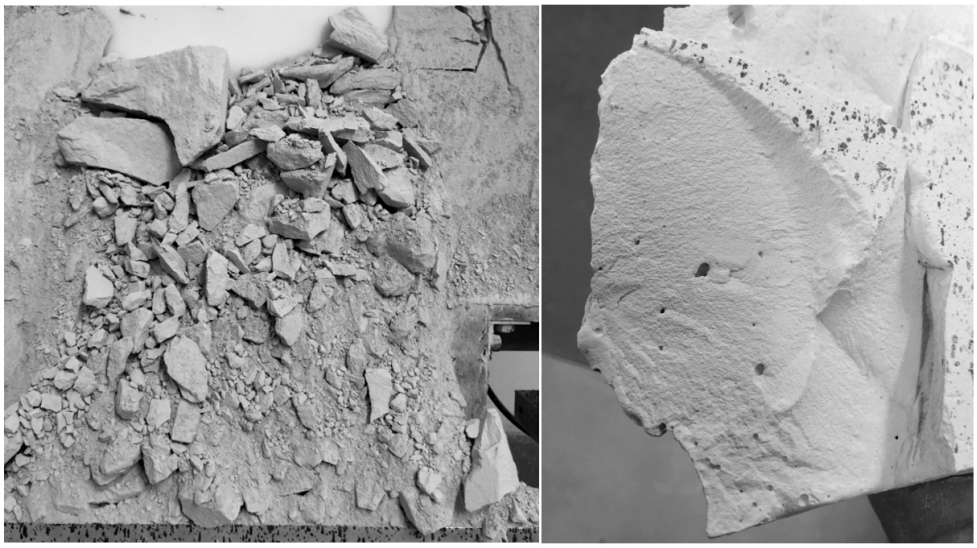

Figure 13 Example of fragmentation of the model material. The left- and right-hand side images are about 30cm and 10cm wide, respectively

5 Observed mechanisms

Similar cave propagation mechanisms were observed in different centrifuge tests. The mechanism dominating the cave propagation in the tests was the generation and extension of tensile/extensile fractures with secondary shearing on structures and through the mass. The fractures were often initiated in the crown of the cave, where the major principal stress acted horizontally due to the stress concentration of the horizontal stress, and extended outward sub-parallel to the cave back to form beams, which then failed onto the caved material. The fracture appeared to initiate and grow in the plane of the major and intermediate stress normal to the minor principal stress direction. Thinner beams formed by extension fracturing failed in bending and flexural shear on the abutments, with bigger blocks shearing on the abutment. The primary fragmentation contained large blocks, which broke down with downward migration. The possibility that extension fracturing makes a much greater contribution to the caving process than previously anticipated was flagged by Cumming-Potvin et al. (2016a) but previously, due to relatively large image intervals, the existential nature of many of the fractures could not be confirmed.

Figure 14 illustrates the mechanisms observed at different stages for one of the tests. Fractures that initiated in a purely dilatant manner with no observable shearing component are highlighted as black lines. Discontinuities with a strong shearing action when first observed are shown as red lines. Blue lines are fractures with an unclear mechanism. White dashed lines denote pre-existing cracks. Also visible in this test is a crack in the glass panel and its shadow on the sample marked with "*" and "#" respectively in sub-figure a. This crack was limited to the centre pane of the three glass panes and did not influence the results.

Figure 14a) shows the initial collapse with a beam forming above the cave back as an extension fracture (2) formed sub parallel to the cave back. It is important to note that the visible fracture did not at this stage reach the undercut level. This beam (α) collapsed in a bending motion, which was followed by the creation of an extension fracture (3) sub-parallel to the cave back. After this beam, a new extension fracture (2) was visible (sub-figure b). This fracture was first visible as two unconnected shorter fractures that connected with further fracture growth. Higher up, another extension fracture was formed (4) with two unconnected shorter fractures (5) formed closer to the abutment. These shorter fractures connected to each other and with fracture 4 as with further fracture growth. In sub-figure c, fracture (6) was not connected with fractures (4-5). With further extension, fractures (4-5) and (6) intersected to form a large block (β). Block (β) was subject to a cantilever bending motion resulting in further fracturing of the block as fracture 4 extended left to intersect the pre-existing discontinuity and a further fracture created to the left of the pre-existing joint formed beam (γ) (sub-figure d). Beam (γ) failed with a cantilever action with shearing along fracture (9). Two new extension fractures (10) formed in the crown of the cave, connecting

with each other and growing towards the right hand abutment to form beam (δ) (sub-figure e and f). Beam (δ) deformed with a cantilever motion with dilation on fracture (10) and shearing on fracture (11). The sub-horizontal, pre-existing fracture above the cave influenced the formation of the fractures to create a disproportionately large block with the growth of fracture 12 and 13. The mechanism of fracture 1 was uncertain whilst fracture 13 appeared to be shearing. Fracture 14 formed internally to block (ε) creating a smaller beam (η). It is not clear from the images whether block (ε) or beam (η) formed first. Fracture 14 grew further towards the left (sub-figure h) and failed in a flexural bending mode leaving cantilever block θ. With further draw all the blocks, including block (ε), underwent secondary breakage to substantially smaller particles.

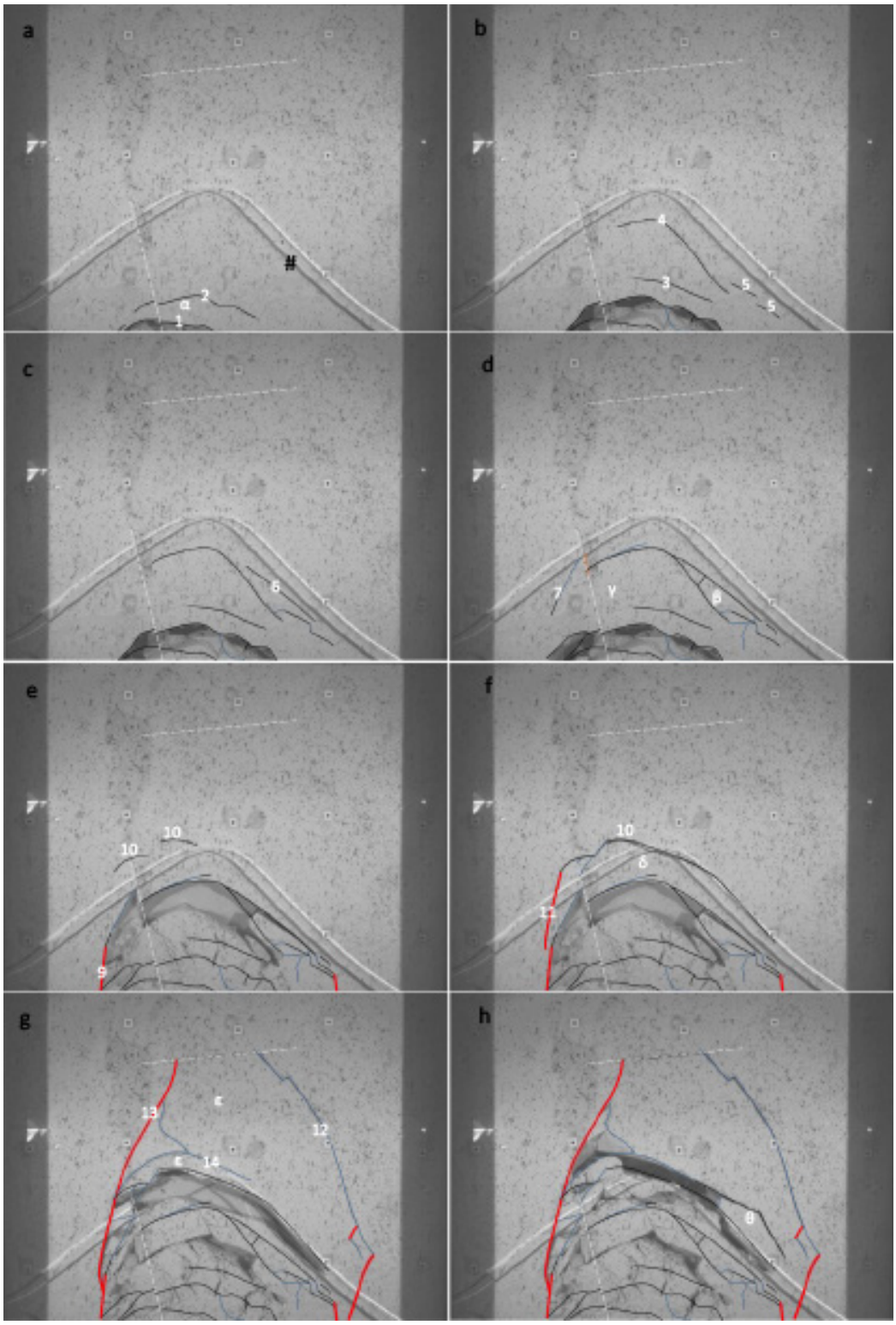

Figure 14 Cave progression with observed extension fractures highlighted in black, shear fractures in red and fractures with unclear mechanism in blue

6 Discussion

The successful execution of physical modelling for rock mechanics problems and especially for the caving scenario is both difficult and complex. The range of scenarios and the ease with which these could be executed is limited compared to numerical models. The value of the physical tests, however, lies in the fact that they are physical – observed behaviour is the direct result of natural physical processes. Due to the practical constraints of the physical models, none of the models can be regarded as being equivalent to a real underground cave. It is important to note that the intention of the models performed in the testing programme, of which a small sub-set is presented here, is not to replicate a particular real cave – but to study the mechanisms involved in cave propagation with horizontal stress concentration and vertical stress relaxation above the cave.

The physical modelling programme highlights important mechanisms and provides the opportunity for direct observation of these mechanisms. A data-rich laboratory environment allows for deeper investigation into these mechanisms and provides well-documented cases against which to validate and improve numerical material models and numerical modelling approaches. Numerical modelling of physically modelled scenarios allows for direct comparison and renders some of the physical model limitations and simplifications unimportant as the numerical model should include those same limitations and should capture the same mechanisms under the modelled conditions.

Planned improvements to future physical modelling include the further improvement in the material model, the extension of the range of horizontal stress conditions, and the measurement of the out-of-plane stress.

7 Concluding remarks

Due to the nature of cave mining, the industry needs to rely on indirect data and limited direct observation to investigate the mechanisms and processes of cave propagation. In addition to field observations, Centrifuge laboratory models are necessary to study the caving process as this provides the opportunity to create a data-rich environment to improve our understanding and validate and extend numerical methods.

The mechanism of cave propagation in the centrifuge is dominated by primary extension fracturing initiating in the cave crown, where higher horizontal stress and low vertical stress occur. The fractures were observed to extend sub-parallel to the cave back, with secondary shear fractures forming. Shear fractures occurred predominantly on the side of the cave closer to the abutment where a higher confinement due to the cave column was still present.

Acknowledgement

The authors would like to thank Newcrest Mining Limited for sponsoring this research.

References

Brown, ET 2007, 'Block Caving Geomechanics, Julius Kruttschnitt Mineral Research Centre', The University of Queensland. Second edition. p. 516

Bucky, PB 1931, 'Use of models for the study of mining problems', American Institute of Mining and Metallurgical Engineers', Technical Publication, no. 425, pp. 3-28.

Bucky, PB & Fentress, AL 1934, 'Application of principles of similitude to design of mine workings', American Institute of Mining and Metallurgical Engineers, Technical Publication, no. 529, pp. 3-20.

Bucky, PB, Solakian, AG & Baldin, LS 1935, 'Centrifugal method of testing models', Civil Engineering, vol. 5, no. 5, pp. 287-290.

Cumming-Potvin, D 2018, 'An Extended Conceptual Model of Caving Mechanics'. PhD, The University of Western Australia.

Cumming-Potvin, D, Wesseloo, J, Jacobsz, SW & Kearsley, E 2016a, 'Fracture banding in caving mines', Journal of the Southern African Institute of Mining and Metallurgy, vol. 116, no. 8, pp. 753-761.

Cumming-Potvin, D, Wesseloo, J, Jacobsz, SW & Kearsley, E 2016b, 'Results from Physical Models of Block Caving', in C Carr & G Chitombo (eds), Proceedings of MassMin 2016, Sydney, New South Wales, Australia, Australian Institute of Mining and Metallurgy, Australia, pp. 329-340.

Duplancic, P & Brady, BH 1999, 'Characterisation of Caving Mechanisms By Analysis of Seismicity And Rock Stress', 9th ISRM Congress, 1999, Paris, France, International Society for Rock Mechanics and Rock Engineering.

Güney, MS, Tayfur, G, Bombar, G & Elci, S 2014, 'Distorted Physical Model to Study Sudden Partial Dam Break Flows in an Urban Area', Journal of Hydraulic Engineering, vol. 140, no. 11, pp. 05014006.

Hoek, E 1965, 'The design of a centrifuge for the simulation of gravitational force fields in mine models', Journal of the Southern African Institute of Mining and Metallurgy, vol. 65, no. 9, pp. 455-487.

Jacobsz, SW, Kearsley, EP, Cumming-Potvin, D & Wesseloo, J 2018, 'Modelling cave mining in the geotechnical centrifuge', in Andrew McNamara, Sam Divall, Richard Goodey, Neil Taylor, Sarah Stallebrass & J Panchal (eds), Physical Modeling in Geotechnics, The 9th International Conference on Physical Modelling in Geotechnics (ICPMG 2018), 2018, London, United Kingdom, CRC Press, pp. 809-814.

Kumcu, SY 2017, 'Investigation of flow over spillway modeling and comparison between experimental data and CFD analysis', KSCE Journal of Civil Engineering, vol. 21, no. 3, pp. 994-1003.

Lambe, TW 1973, 'Predictions in Soil Engineering', Géotechnique, vol. 23, no. 2, pp. 149-202.

Torres Mansilla, C 2018, 'Numerical Modelling of Hydraulic Free Surface Flows and Scale Effects Associated with Physical Modelling'. University of Leeds.